Progress in Organic Coatings 177 (2023) 107428

Contents lists available at ScienceDirect

Progress in Organic Coatings

journal homepage: www.elsevier.com/locate/porgcoat

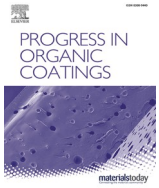

Sustainable biocarbon/tung oil coatings with hydrophobic and UV-shielding properties for outdoor wood substrates

Laetitia Marrot [a,b,c,*], Mariem Zouari [b,c], Matthew Schwarzkopf [b,c], David Brian DeVallance [b,c,d]

[a] FRISSBE, Slovenian National Building and Civil Engineering Institute (ZAG), 1000 Ljubljana, Slovenia
[b] Innorenew CoE, Livade 6, 6310 Izola, Slovenia
[c] Faculty of Mathematics Natural Sciences and Information Technologies, University of Primorska, Muzejski Trg 2, 6000 Koper, Slovenia
[d] College of Science and Technology, Commonwealth University, 401 North Fairview Street, Lock Haven, PA 17745, United States

ARTICLE INFO

Keywords:
Biocarbon
Biochar
Coating
Wood protection
Hydrophobic coating
Wettability

ABSTRACT

With wood regaining substantial interest as a construction material due to sustainability concerns and aesthetics trends, efficient and safe protection methods are needed to prevent the discouloration and the loss of mechanical properties of this renewable and UV-sensitive material. In this study, sustainable coatings comprising 0 to 20 wt % biocarbon (BC) dispersed in tung oil were developed for wood protection. BC particles were added as ultraviolet (UV) absorbers and were produced by various carbonization routes. The BC powders were characterized in terms of particle size and surface functional groups by Fourier-Transform infrared, and the UV and visible absorbance of dispersed BC powders in water solutions were related to these characteristics.

Two wooden substrates (beech and oak) were coated with the developed coatings and the samples underwent six months of onsite weathering. While the total colour change of uncoated samples and tung oil-coated substrates without BC kept increasing over time and resulted in a clear alteration of the wood surface aesthetics, an increased BC content in the coatings led to enhanced colour stability, with alteration of the colour close to 2 for both wood species after six months of weathering for 10 and 20 wt% BC.

Coating with tung oil made the wooden substrates, initially hydrophilic, become hydrophobic, and the further introduction of biocarbon increased hydrophobicity. However, the increase in BC content was not correlated with an increase in water repellence, the highest water contact angle being observed for 5 % BC, and no further improvement in hydrophobicity was observed with higher BC content. The weathering negatively affected the water repellence of all the samples (i.e., reference samples and coated samples with various BC content). However, the introduction of 20 % BC best protected the decrease in water repellence induced by the onsite weathering.

1. Introduction

Wood as a construction material has regained substantial interest due to sustainability concerns and aesthetics trends. However, as a biobased material, wood is sensitive to humidity and ultraviolet (UV) radiation, which triggers the formation of free radicals and induces depolymerization of its lignin and cellulose components [1]. Outdoor exposure of wooden materials can result in swelling, mould and fungi attacks, discolouration, yellowing, and loss of gloss and mechanical properties [2,3]. UV-protective agents are needed to preserve wood from the deterioration linked to UV exposure. Synthetic organic and inorganic UV filters have been developed and massively commercialized for various markets. Due to their release into the aquatic environment, organic UV filters are becoming an essential group of emerging contaminants, raising concerns about their impact on the environment and human health [4]. Inorganic UV absorbers based on metal oxide semiconductors (such as TiO_2, ZnO, SiO_2 and Al_2O_3 [5]) appear less toxic and chemically more stable than organic absorbers when exposed to high temperatures and UV. However, some inorganic UV absorbers started showing safety concerns recently. For example, the European Union published in 2020 the official delegated regulation to classify TiO_2 as a suspected carcinogen by inhalation. Hence, further research is needed to develop efficient but safer and more sustainable UV absorbers.

Carbon-based materials in different forms (e.g., carbon black [6,7],

* Corresponding author at: FRISSBE, Slovenian National Building and Civil Engineering Institute (ZAG), 1000 Ljubljana, Slovenia.
E-mail addresses: laetitia.marrot@zag.si (L. Marrot), mariem.zouari@innorenew.eu (M. Zouari), matthew.schwarzkopf@innorenew.eu (M. Schwarzkopf), ddevallanc@lockhaven.edu (D.B. DeVallance).

https://doi.org/10.1016/j.porgcoat.2023.107428
Received 21 November 2022; Received in revised form 23 December 2022; Accepted 12 January 2023
Available online 25 January 2023

graphite [8], diamond [8], carbon nanotubes [9]) have been studied for use as polymer UV stabilizers because of the combined effects of the physical screen, UV absorption, and radical trap, while providing sustainable and consumer accepted solutions. However, while carbon black displayed satisfying UV protection of polymers, graphite and diamond were found to enhance photooxidative degradation of polyethylene films exposed to simulated sunlight, even though they are effective light shields [8]. Literature also reports the use of carbon-based materials in coatings for wooden substrates. Yuan et al. [10] prepared a transparent, metal-free UV coating using graphitic carbon nitride nanosheets as UV absorber and cellulose nanofibrils as a film forming carrier. The coating presented UV-shielding and hydrophobic properties brought by a thermal chemical vapor deposition process. Łukawski et al. [11] investigated the possibility of using carbon black, graphene and carbon nanotubes as water-repellent agents for wooden substrates. They obtained homogeneous carbon nano-materials, organic solvents or water coatings with apparent hydrophobicity. However, the authors did not evaluate any UV protection properties of the coatings.

While fossil-based carbons can be used as UV-resistant coatings, bio-based carbon would provide a more sustainable carbon source. Biocarbon (BC) is a carbon-based product obtained from the carbonization (slow pyrolysis process) of organic materials in the absence of oxygen at temperatures above 300–400 °C [12]. Low-cost organic materials can be acquired as side streams from the agricultural or forestry industries and be efficiently converted into BC. BC has gained scientific interest thanks to its utilization in environmental management and its ability to mitigate greenhouse gas emissions, such as sequestration of CO_2 and CH_4 in global carbon pools, and to mitigate N_2O emissions, the most critical ozone-depleting compound in the atmosphere [13]. The BC properties (i.e., size and extension of the porosities, ash content, carbon content and structure) can be optimized by adapting the production process parameters to target specific applications (e.g., absorption, electrical conductivity and soil amendment). BC from various biomass has recently shown promising light-absorbing properties for solar-steam generation devices [14–18]. This application, though, focuses on wavelengths ranging between 400 nm and 2500 nm and does not consider the UV radiation range. In another study, Chatzimitakos et al. [19] highlighted the UV protection properties of algae-derived carbon nanodots, making them promising for sunscreen formulations.

As sustainable film formers, drying oils are extracted from plants, crosslinking at contact with the oxygen in the air. One popular drying oil in Asia and America is tung oil, extracted from the tung tree's nut (*Vernicia fordii*). Tung oil consists of conjugated triene-dominated fatty acid that polymerizes faster than the non-conjugated double bond systems (e.g. linseed oil). This formulation results in hydrophobicity shortly after being applied to wood [20]. Tung oil is used to protect wood thanks to its water-repellent properties. Along with the water-repellent effect, Humar and Lesar [21] highlighted tung oil's brown- and white-rot fungi protection, and the short-, medium-, and long-term water uptake prevention. However, pure tung oil's relatively long drying time (longer than five days) limits its industrial application or requires drying agents to be added to its formulation. For example, Yang et al. [22] have shown that the curing can be reduced to a few hours using a combination of catalysts.

Given the promising use of BC for UV protection, in this study, we aimed develop affordable and sustainable wooden coatings for façades or other outdoor applications. Specifically, we developed sustainable coatings comprising of 0 to 20 wt% BC dispersed in tung oil for wood protection. Two wood species were selected to evaluate the influence of the wooden substrate on the results. We investigated the effect of hemp-derived BC particles on the hydrophobicity and UV protection of the coated wooden substrates. The carbonization process parameters for BC production were monitored and related to the UV protection efficiency of the resulting carbon materials.

2. Material and methods

2.1. Hemp biomass carbonization and characterization of hemp-derived biocarbon (BC)

Hemp (*Cannabis sativa* L.) stems from the Futura 75 variety, grown in 2020 in Frankolovo (Slovenia), were supplied by the Vrhivšek farm. The stems were cut into 10 cm segments and stored in a dry environment before undergoing a carbonization process via a tube furnace (Nabertherm RSRC 120-1000/13, Nabertherm, Lilienthal, Germany) under an inert nitrogen flow rate of 300 L/h. Hemp derived biocarbon (BC) samples were prepared following ten different thermochemical conversion routes, as described in Table 1, to evaluate the influence of the process parameters on the visible and UV absorbance of the BC.

Following the thermochemical conversion, the hemp-derived BC from each batch was manually crushed and transferred to stainless steel jars with 20 mm diameter stainless steel balls (balls to BC ratio was equal to 25). The BC was then ballmilled in deionized water for 30 min at 400 rpm with a planetary mill (Pulverisette 5, Fritsch, Idar-Oberstein, Germany). Thirty milling cycles (1 min on, followed by 5 min off) were repeated to avoid temperature rise. The ballmilling parameters (solvent, ratio of milling media:BC, milling time and resting period) were optimized to obtain BC particles as small as possible, using the same methodology as Peterson et al. [23]. After milling, the BC samples were transferred into Petri dishes and placed in the oven at 105 °C to allow water evaporation and to obtain BC powder.

For each batch, BC composition in terms of moisture, fixed carbon, volatiles and ash content, and elemental compositions, were reported earlier in [24]. The particle size of the different BC was measured to check the homogeneity of the powders and validate the ball milling efficiency to downsize the particles. Particle size measurements were done with a particle size analyser (Horiba Scientific LA-960A2, Horiba, Kyoto, Japan) in water suspension after 1 min of ultrasound to ensure proper dispersion of the particles. The particle refractive index was taken at 1.920. Ultra-violet (UV) and visible extinction of water solution containing 125 and 250 mg/L of BC were assessed with UV-VIS Spectrophotometer UV7 (Mettler Toledo, Greifensee, Switzerland). Surface functional groups were analyzed by Fourier transform infrared (FTIR) spectroscopy using an ALPHA FT-IR Spectrometer (Bruker, Billerica, MA, USA) equipped with an ATR (attenuated total reflection) module. The absorbance spectra were recorded over a wavelength range from 400 to 4000 cm^{-1}, at 4 cm^{-1} resolution; each spectrum represents an average of 32 scans. The average spectra were then collected, and OPUS software was used for spectra treatment by smoothing and eliminating CO_2 and atmospheric water vapor effects.

Table 1
Different thermochemical conversion routes followed to produce hemp-derived BC.

BC samples	Heating ramp (°C/h)	Pyrolysis temp (°C)	Pyrolysis duration (min)
P400-R200-T30	200	400	30
P600-R200-T30	200	600	30
P800-R200-T30	200	800	30
P1000-R200-T30	200	1000	30
P600-R2000-T30	2000	600	30
P800-R2000-T30	2000	800	30
P1000-R2000-T30	2000	1000	30
P600-R2000-T60	2000	600	60
P800-R2000-T60	2000	800	60
P1000-R2000-T60	2000	1000	60

2.2. Preparation and characterization of the wood coatings

Oak (*Quercus robur*) and European beech *(Fagus sylvatica* L.*)* substrates with dimensions 150 × 150 × 20 mm^3 were selected to apply the coatings by brushing. The moisture content of beech and oak wood was determined in accordance with ISO 3130 standard. Three samples from each wood species were conditioned in a climatic chamber (Kambič KK-8000 CH-2, Semič, Slovenia) for 24 h at 65 % relative humidity and 20 °C. After conditioning, samples were weighed, and initial masses were recorded. Then, samples were oven-dried at 105 °C until achieving constant weight. The moisture content was determined using Eq. (1).

$$Moisture\ content\ (\%) = \frac{m_i - m_d}{m_d} \times 100 \quad (1)$$

where m_i and m_d correspond to initial and dried mass of the sample. The moisture content in beech and oak wood were 8.35 ± 0.15 % and 8.29 ± 0.07 %, respectively.

Density was determined by dividing the initial mass by the volume of the samples. The density of beech and oak wood were 724 $kg.m^{-3}$ and 655 $kg.m^{-3}$, respectively.

BIOHEL tung oil (Helios TBLUS doo, Domžale, Slovenia) was used as a film former for the coating formulations. The BC powders presented in the previous section were mixed for further introduction into the tung oil. Different tung oil-based coating formulations were prepared by dispersing BC particles in tung oil with various ratios (0, 5, 10 and 20 wt % regarding the oil weight). After applications, coatings were left to dry for 4 weeks in a conditioning room at 20 °C and 60 % relative humidity. After drying, each wooden substrate was cut into two pieces of 75 × 150 × 20 mm^3. The edges of all the samples were covered by an impermeable resin to present humidity from penetrating through the sides. Half of the samples were then fixed on a support to be exposed to natural weathering (later referred as weathered samples), while the other half was stored in a drawer, protected from humidity and light (non-weathered samples). In addition, uncoated oak and beech substrates were included in the study (reference samples). Natural weathering was performed for six months on the rooftop of the research center (coordinates 45.53025373745809, 13.656996645911137) from the 1st of September 2021 to the 1st of March 2022 (180 days).

The properties of the coatings (structure, surface colour and wettability) were measured monthly. Before the measurements, weathered samples were conditioned for 24 h in a conditioning room at 20 °C and 60 % relative humidity. The evolution of the surface colour was followed by measuring the lightness, red/green and yellow/blue components in the CIELAB L*a*b* system with a Spektromaster 565–45 spectrophotometer (Erichsen, Hemer, Germany). A D65 illuminant and 10° viewing angle were selected for the measurements. The reported colour values are the average of three different spots. The total colour change ΔE at a given time is given by the Eq. (2). ΔE is measured on a scale from 0 to 100, where 0 is less colour difference, and 100 indicates complete distortion.

$$\Delta E = \sqrt{(\Delta L^*)^2 + (\Delta a^*)^2 + (\Delta b^*)^2} \quad (2)$$

where: L* represents lightness, with 100 being white and 0 being black; a* refers to the red (positive a* values)/green (negative a* values) coordinate; b* refers to the yellow (positive b* values)/blue (negative b* values) coordinate; and ΔL, Δa, Δb correspond to differences between colour coordinate values measured at a given time and referenced to the corresponding value of the initial colour.

The wettability of the coatings was evaluated by wetting the surface with distilled water and measuring the dynamic contact angle with an Attension Theta Flex Auto 4 optical tensiometer (Biolin Scientific, Gothenburg, Sweden) equipped with a 3D Topography Module. Five measurements were performed on each specimen, with a volume of each drop set at 4 μL. Additionally, the transverse plane of the specimens and coatings were assessed before and after six months of weathering. A 5 mm was cut from the end of the specimens to avoid evaluating the end penetration of coatings. This new face was then polished using a rotary sander. The exposed surface and cross-sections were observed with a digital microscope Keyence VHX-6000 (Keyence corporation, Itasca, IL, USA). A piece of paper was affixed to the wood's surface of the wood immediately before imaging to enhance the black surface coating contrast in the cross-section.

3. Results and discussion

3.1. Biocarbon performance as UV and visible light absorber

The particle diameter at 10 % (D10), 50 % (D50) and 90 % (D90) of the cumulative size distribution and the mean size of the BC powders are listed in Table 2.

Independent of the thermochemical conversion route, the overall particle size distribution of the different BC powders was similarly fitted in the micro-size range, with the smallest and highest mean size being 10.8 μm and 37.5 μm, respectively. Nan and DeVallance [25] reported an average mean diameter at 22.9 μm with a normal particle size distribution ranging from 0.5 to 300 μm for their ball milled hardwood BC. In the present study, the ball milling effectively reduced and homogenized the BC particle size, whose distribution range was narrower than in the mentioned reference. However, D90 ranged between 14.6 and 82.7 μm (more than five times higher), and D50 ranged between 9.2 and 21.4 μm (more than two times higher). No correlation was evident between the process parameters (pyrolysis temperature, heating rate and residence time) and the particle size.

The evolution of the biomass degradation with increasing pyrolysis temperature can be seen by comparing the FTIR spectrum of the raw hemp biomass with the spectra of its derivative BC powders (Fig. 1).

Similar spectra were obtained for a given pyrolysis temperature (i.e., for all the BC carbonized at 400 °C, 600 °C, 800 °C, and 1000 °C) regardless of the selected heating rate or residence time. Moreover, the spectra of the BC samples carbonized at 800 °C and 1000 °C were similar.

In the hemp raw biomass spectra, the wideband at about 3300–3450 cm^{-1} corresponded to hydroxyl (—OH) vibrations from water molecules and other OH groups in the sample [26,27]. This band disappeared for the BC samples due to the evaporation of components containing —OH groups during pyrolysis, such as water, alcohol and phenols [28]. The band between 2850 cm^{-1} and 2920 cm^{-1} was assigned to the CH_2 stretching vibrations [29]. This band progressively faded in the BC spectra as pyrolysis temperature increased, along with the degradation of the main hemp constituents (i.e., hemicelluloses, celluloses, and lignin). Similarly, the peak visible in the raw hemp spectra at 1750 cm^{-1} corresponding to C═O carbonyl groups diminished in intensity for the BC samples carbonized at 400 and 600 °C and completely disappeared at 800 and 1000 °C. Deterioration of the natural polymers was also

Table 2
Particles' size and representative diameters of the BC.

BC samples	D10 (μm)	D50 (μm)	D90 (μm)	Mean size (μm)
P400-R200-T30	6.5 ± 2.6	21.4 ± 0.5	82.7 ± 3.1	37.5 ± 2.1
P600-R200-T30	6.7 ± 3.1	9.8 ± 1.3	25.2 ± 10.6	15.9 ± 5.4
P800-R200-T30	3.7 ± 1.0	9.2 ± 2.0	14.6 ± 4.8	10.8 ± 3.1
P1000-R200-T30	3.1 ± 0.1	11.5 ± 0.2	27.9 ± 6.9	20.8 ± 2.8
P600-R2000-T30	4.1[a]	11.4[a]	40.1[a]	34.0[a]
P800-R2000-T30	3.1[a]	12.5[a]	65.4[a]	27.5[a]
P1000-R2000-T30	2.9 ± 0.1	11.3 ± 1.0	49.5 ± 1.5	20.5 ± 0.1
P600-R2000-T60	3.3 ± 0.1	10.5 ± 0.1	23.1 ± 0.7	28.1 ± 1.3
P800-R2000-T60	3.2 ± 0.3	10.6 ± 0.8	15.7 ± 4.6	15.0 ± 7.5
P1000-R2000-T60	2.9 ± 0.0	10.8 ± 0.4	39.3 ± 15.3	21.0 ± 7.3

[a] Only one measurement was performed instead of the average of three repetitions.

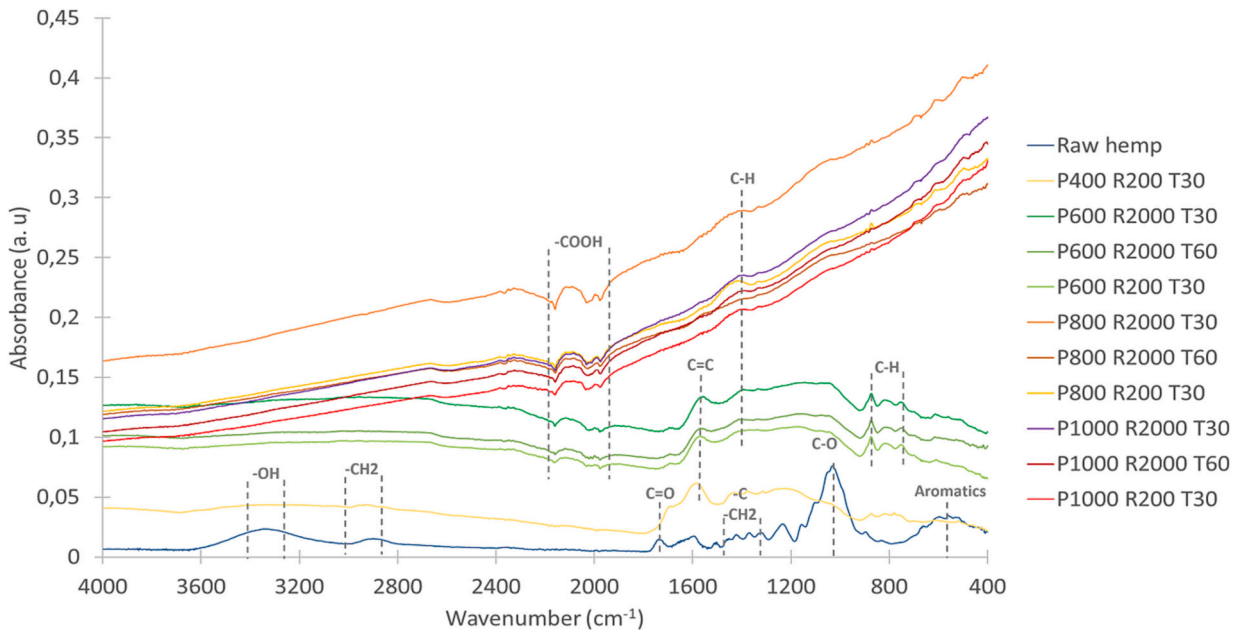

Fig. 1. FTIR spectra of the BC powders and hemp raw biomass precursor. Figure in colour online only.

evidenced by the disappearance of the peaks from the hemp spectrum to the BC spectra, between 1400 cm^{-1} and 1500 cm^{-1} corresponding to aromatic C and aliphatic CH_2— groups present in lignin polymers [30], and the band at 1385 cm^{-1}, corresponding to aromatic C—H stretching. Moreover, the band at 1050 cm^{-1}, attributed to the C—O stretching in cellulose and hemicellulose [31], was visible only in the raw hemp spectrum. The large peak of around 570 cm^{-1} obtained for raw hemp corresponds to aromatic rings [32] that might be derived from lignin polymers. This band was no more visible in the BC spectra due to the thermal degradation of lignin during the carbonization process. In the BC spectra, a wide band ranging between 1900 cm^{-1} and 2200 cm^{-1}, assigned to carboxyl vibrations [33], gradually appeared (not present for a 400 °C pyrolysis, visible from 600 °C and above, and stronger for pyrolysis at 800 °C and 1000 °C). Shafizadeh et al. [34] observed that the mainly aliphatic carbon structures in the polymer units of cellulose changed after pyrolysis to a mix of aliphatic, alkene, aromatic, carboxylic and carbonyl carbon structures, which justify the rise of carboxyl groups found in the BC powders. The band at 1580 cm^{-1}, related to the occurrence of C=C bonds with conjugation of π electrons [35] and linked to the presence of alkenes and aromatics [36], was weak for the hemp biomass, intensified for BC at 400 and 600 °C, and then disappeared for BC at 800 and 1000 °C. Additionally, aromatic hydrogen structures (C—H stretching [31,33]) were detected near 740 cm^{-1} and 870 cm^{-1} in the BC spectra for the powders carbonized at 400 and 600 °C, while these bands were absent in the raw hemp spectrum. The FTIR spectra highlighted the progressive changes of functional groups appearing in hemp biomass undergoing carbonization, indicating the dehydration and degradation of lignocellulosic components, the appearance of their transformation derivatives and the increase in aromatic carbon structures.

The absorbance of water solutions containing the dispersed BC particles produced by the different thermochemical conversion routes was measured in the UV and visible range (wavelength from 300 to 800 nm). Two concentrations were selected (125 and 250 mg/L), with higher concentrations leading to the detector's saturation with absorbance values largely above 1. For both concentrations and for all the different BC considered, the absorbance was roughly constant in the UV and visible range of the spectra, slightly increasing with an increase in the wavelength.

Table 3 shows the absorbance values at 300 nm and 800 nm for all the BC samples. For each sample, the absorbance at the two chosen wavelengths was systematically doubled when the concentration was doubled. This result highlights a direct proportion between the concentration of the solution and its absorbance. Chatzimitakos et al. [19] similarly found a direct proportion between the concentration of algal-based carbon nanodot solutions and the corresponding sun protection factor in the UV-B region (290–320 nm), with an average nanodot particle size of 3 nm.

Table 3
Absorbance values of the different BC water solutions at 125 mg/L and 250 mg/L.

Concentration	125 mg/L		250 mg/L	
BC samples	$A_{\lambda=300\ nm}$	$A_{\lambda=800\ nm}$	$A_{\lambda=300\ nm}$	$A_{\lambda=800\ nm}$
P400-R200-T30	0.34	0.37	0.58	0.68
P600-R200-T30	0.32	0.37	0.62	0.73
P800-R200-T30	0.35	0.41	0.70	0.82
P1000-R200-T30	0.36	0.38	0.70	0.78
P600-R2000-T30	0.42	0.49	0.81	0.95
P800-R2000-T30	0.41	0.50	0.85	0.98
P1000-R2000-T30	0.42	0.46	0.80	0.90
P600-R2000-T60	0.43	0.51	0.88	1.03
P800-R2000-T60	0.41	0.45	0.77	0.87
P1000-R2000-T60	0.34	0.36	0.65	0.73

The absorption mechanisms of light-absorbing carbon have been thoroughly described by Bond et Bergstrom [37]. The optical or electronic properties of carbonaceous material depend on their molecular form, and more specifically are governed by the size of sp2-bonded clusters, which are absorbing structures. Increasing sp2-islands size decreases the optical gap and increases absorption [37]. In a previous study [24], we characterized the different BC samples' microstructure to explain their electrical conductivity and highlight changes in microstructure in relation to the pyrolysis temperature. Below 600 °C, amorphous phases predominate in the carbon structure, composed of a mixture of sp2 and sp3 bonds, with no long-range crystalline order. Between 600 and 800 °C, defected graphene structures with sp2-bonded clusters start to appear and densify, decreasing the part of the amorphous phase until a percolation threshold, allowing electron's mobility that kept increasing with the compaction of defected graphene clusters. Between 800 and 1000 °C, graphite-like structures keep growing and

packing, increasing sp2-islands size. The FTIR analysis in Fig. 1 confirmed the rise of C═C bonds with conjugated π electrons and aromatic hydrogen structures in the BC spectra. Hence, from a structural point of view, the absorption of the BC samples should increase with the pyrolysis temperature at which they were produced. However, we did not observe any convincing relationship between the production process parameters of the BC with their absorbance. It may be due to the particle size of the different BC samples. Indeed, for an equivalent concentration, the size of the particles highly influences their absorbance. The higher the particle size, the lower their absorbance. We showed in a previous paper [38] that the smallest fraction (0–20 μm) of beech derived biochar in water solution concentrated at 200 mg/L displayed an absorbance close to 1, while a powder from the same material sieved at 106–150 μm gave an absorbance of 0.7 at 500 mg/L. In this study, despite the desire to obtain a homogeneous particle size through ball milling, the particle size analysis showed some discrepancy from one BC to the other, which most probably disturbed an eventual correlation between absorbance and production parameters.

3.2. Performances of biocarbon/tung oil coatings with various biocarbon content

Pictures of the beech (*Fagus sylvatica L.*) and oak (*Quercus robur*) substrates uncoated and coated with 0, 5, 10, and 20 % BC in tung oil are presented in Figs. S1 and S2, supporting information, respectively. Non-weathered beech and oak samples (top pictures) are compared with six months naturally weathered samples (bottom pictures).

3.2.1. Coating structure

Micrographs of the cross-section of the coatings containing 0 % and 20 % of BC in tung oil are seen in Figs. 2 and 3. In weathered beech specimens with 0 % biochar coatings, surface degradation can be seen in the form of an uneven surface. This degradation is primarily due to uneven UV degradation of earlywood (more degraded) and latewood (less degraded). In specimens with 20 % biochar in the coatings, there is little to no degradation visible on the surface. The penetration of the coating into the wood is most easily seen in those with biochar. However, very little penetration (<0.5 mm) occurred and is seen to penetrate through earlywood vessels.

In oak, little to no penetration was seen except in earlywood vessels that were crosscut and exposed on the coated, tangential face of the specimens. Oak can be difficult to evenly stain or treat due to its large, ring-porous earlywood vessels, which, species dependent, can have tyloses present that block penetration through the vessels. Despite poor penetration, the surface coating appears to have protected the surface from degradation, as seen in Figs. 2 and 3, and Figs. S1 and S2, supporting information.

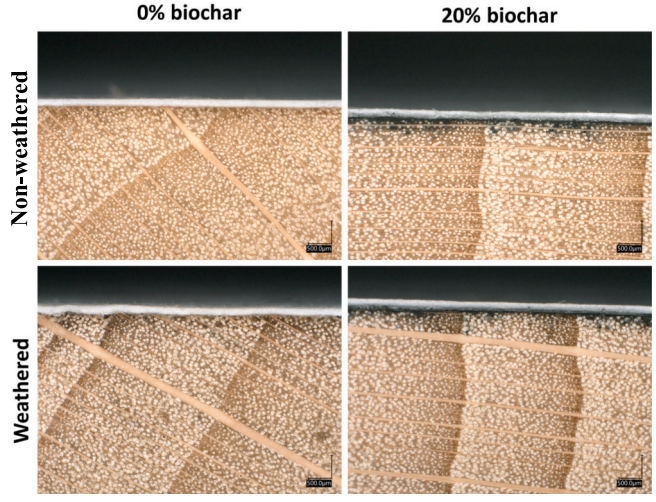

Fig. 2. Beech specimens before and after six months of weathering with 0 % and 20 % BC coatings. Figure in colour online only.

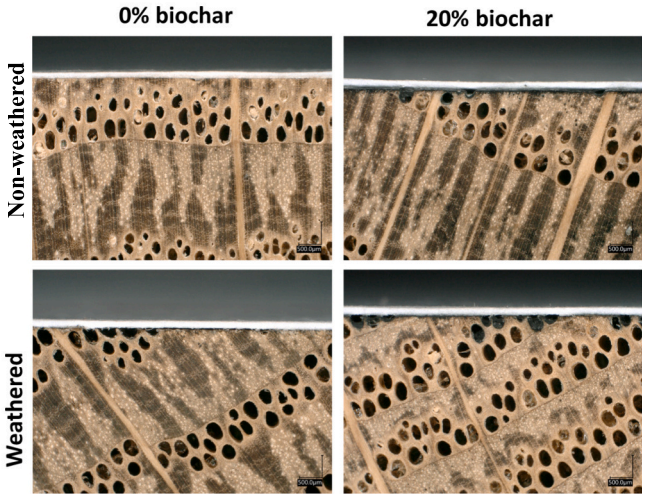

Fig. 3. Oak specimens before and after six months of weathering with 0 % and 20 % BC coatings. Figure in colour online only.

3.2.2. Colour stability

Average values and evolution of L*, a*, b* and total colour change ΔE of the coated beech and oak substrates with onsite weathering time are presented in Figs. 4–7, respectively. Values associated with the figures are reported in Tables S1–S4 of the supporting information.

For both the uncoated beech and oak reference samples, the lightness L* continuously decreased with increasing weathering as shown in a general darkening of the surface (Fig. 4). The lightness corresponding to the beech surface was higher than for oak due to the natural lighter colour of this species (see Fig. S1 for beech and Fig. S2 for oak). With the application of tung oil without BC (0 % BC coating), the lightness was shifted toward darker tones due to the brownish colour of the tung oil. Still, the decreasing trend over weathering time remained, stabilizing to a constant value for the last two points (155 and 180 days). This observation can be explained by the strong UV and visible light absorption of tung oil [39]. Moreover, tung oil coating was found an effective treatment against wood-decay fungi and water uptake [21], slowing down the overall degradation of wood surfaces exposed outdoors. The addition of biochar in the coating (5, 10 and 20 %) sharply lowered the lightness of the coatings (Fig. 4), which remained relatively stable between 19.5 and 24.4 over the weathering time. Poohphajai et al. [40] reported similar CIE L* values ranging from 23.1 to 24.0 for black coatings using biofilms.

The a* and b* values of the control substrates (beech and oak) decreased over the six months of onsite weathering (Figs. 5 and 6), meaning a decrease in the red and yellow colours. Photochemical reactions and/or photooxidation of the wood constituents induced the liberation of chromophoric units and contributed to colour changes on the wood surface. Pandey [41] also highlighted the effects of the presence of extractives on colour changes of wood surfaces. Persze and Tolvaj [42] reported an effect of temperature during photo-degradation. In our study, the difference in extractives content for beech and wood did not noticeably influence the a* and b* values of the reference substrates, which were in the same range regardless of the wood species. Moreover, past research [41,42] reported an increase of a* and b* values with weathering time. In our study, however, the opposite trend was found. The prior referenced studies considered artificial weathering performed with xenon and mercury light sources, whereas the onsite weathering in the current study induces complex phenomena with the combined effect of water, fungi, UV light, oxygen, heat and atmospheric

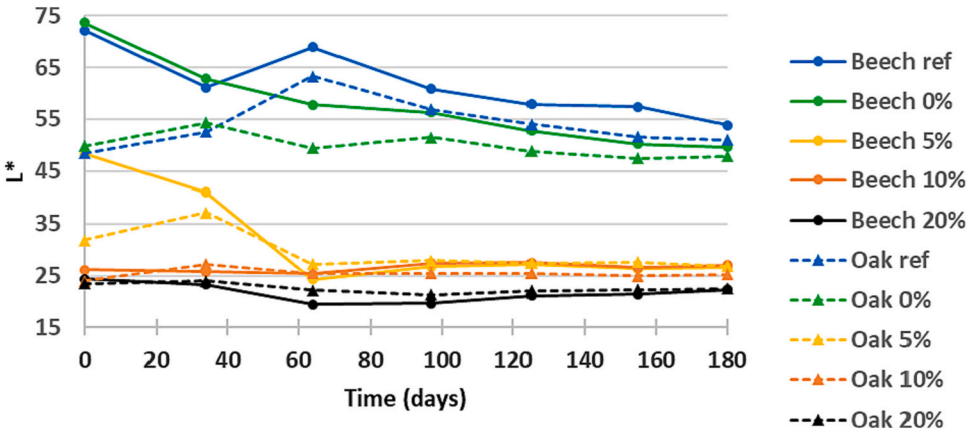

Fig. 4. Evolution of L* of the coated wooden substrates with onsite weathering time. Figure in colour online only.

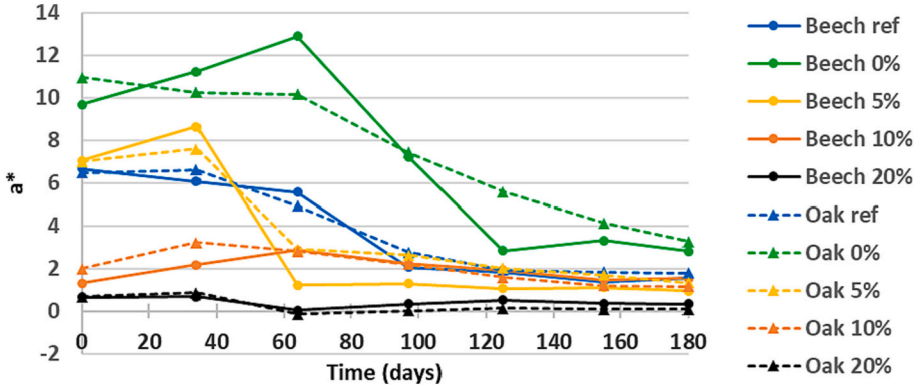

Fig. 5. Evolution of a* of the coated wooden substrates with onsite weathering time. Figure in colour online only.

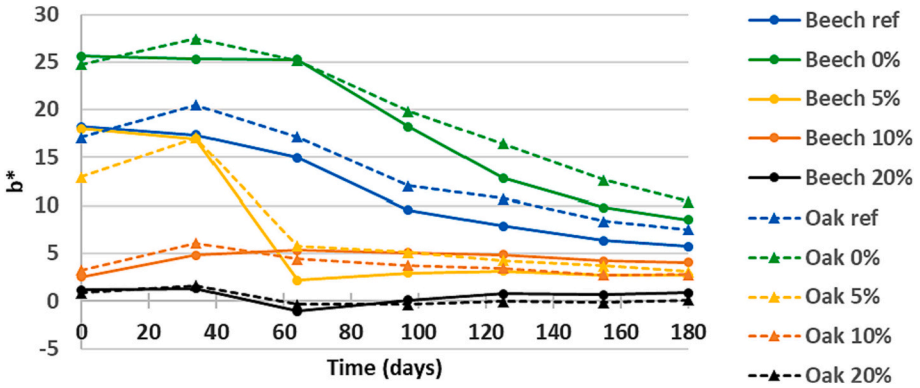

Fig. 6. Evolution of b* of the coated wooden substrates with onsite weathering time. Figure in colour online only.

pollutants. The application of tung oil at the surface of both wood species shifted a* and b* toward higher values but did not change the decreasing trend during weathering. Both a* and b* values decreased with the addition of BC, stabilizing close to zero with 20 % BC for the whole weathering period.

Overall, the total colour change of uncoated and tung oil-coated beech and oak substrates without BC kept increasing over time (Fig. 7), and resulted in a clear alteration of the wood surface aesthetics. Beech was more affected than oak (ΔE close to 30 and 20 at the end of the weathering period, respectively), which can be directly related to the differences in the composition of these two wood species. Indeed, Wang and Ren [43] correlated the total colour changes with lignin degradation and carbonyl formation based on the ratio of lignin/carbohydrate and carbonyl/carbohydrate in FTIR spectra. The wooden substrates protected with pure tung oil resulted in a more remarkable colour change than the uncoated substrates. At the same time, Peng et al. [39] report a strong UV and visible light absorption of tung oil, which should impart higher colour stability to the wood surfaces. However, tung oil is susceptible to providing nutrients for fungi growth [21], and the latter could be responsible for the observed higher colour change. An increased BC content in the coatings led to enhanced colour stability, with alteration of the colour close to 2 for both wood species after six months of weathering for 10 and 20 wt% BC, meaning that the colour change is only perceptible through close observation.

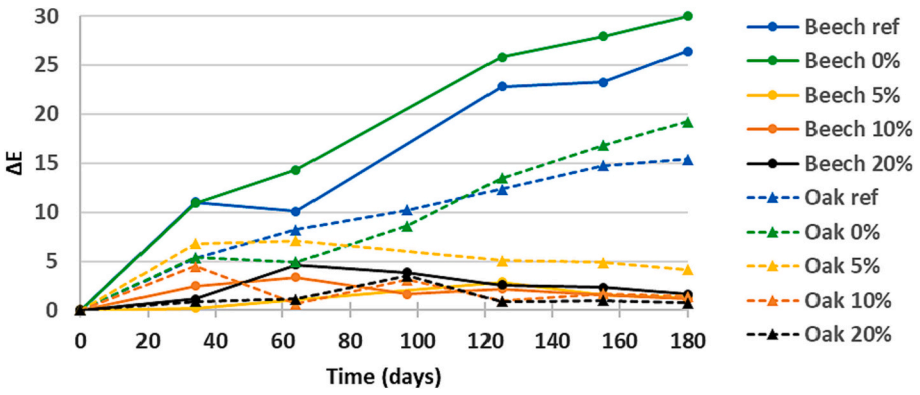

Fig. 7. Evolution of Δ E of the coated wooden substrates with onsite weathering time. Figure in colour online only.

3.2.3. Wettability of the coating

The wettability of the coatings was evaluated by measuring the water contact angle (WCA) at the coating surface. Figs. 8 and 9 show the evolution of the WCA for non-weathered and weathered coatings with onsite weathering time, for beech and oak, respectively. A surface can be categorized as super-hydrophilic when WCA = 0°, hydrophilic when WCA < 90°, hydrophobic when WCA > 90° and super-hydrophobic when WCA > 150° [44]. Initially (day 0), both uncoated (control) beech and oak surfaces showed a hydrophilic character with WCAs around 56° and 81°, respectively. The higher WCA obtained with oak control was likely due to the presence of tyloses which block the penetration of liquids (water) through the vessels. After treatment with tung

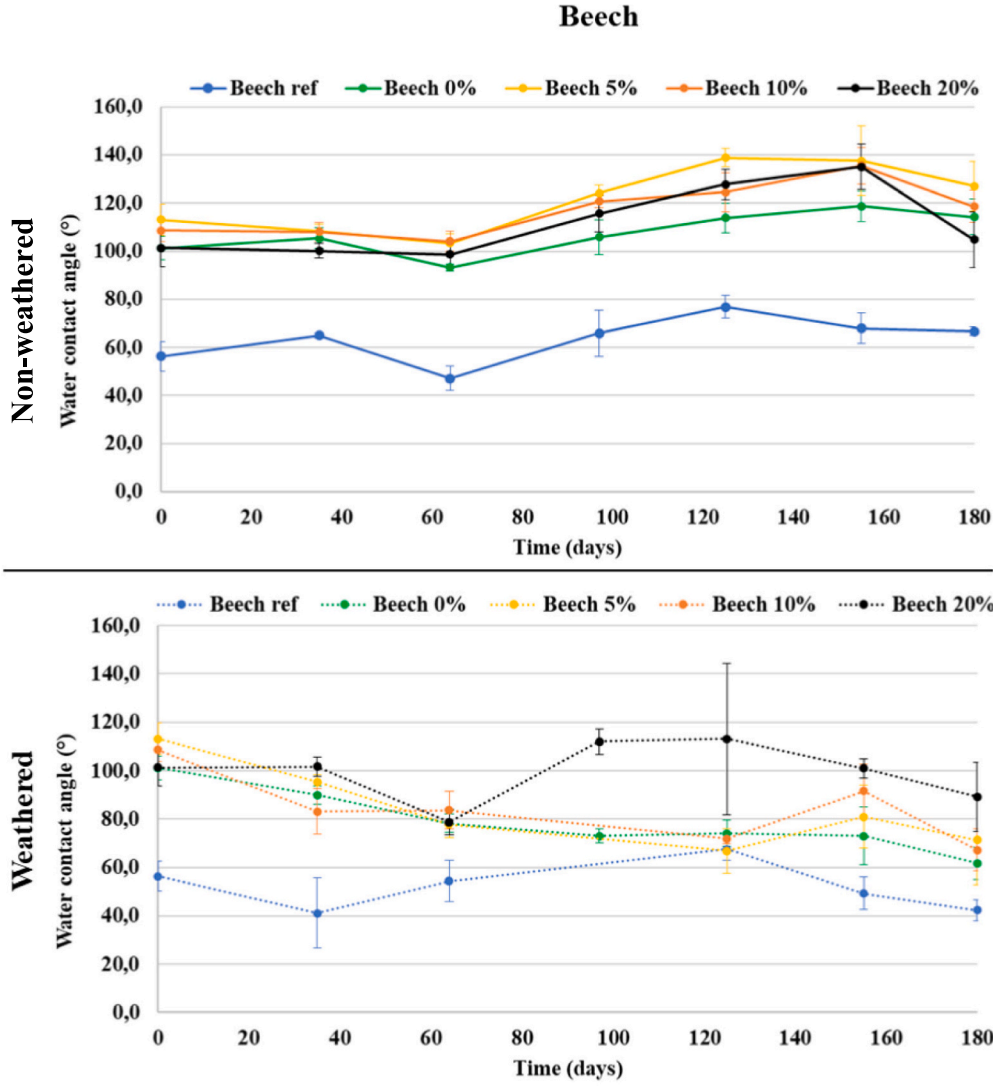

Fig. 8. Evolution of the water contact angle for non-weathered and weathered beech coatings with onsite weathering time. Figure in colour online only.

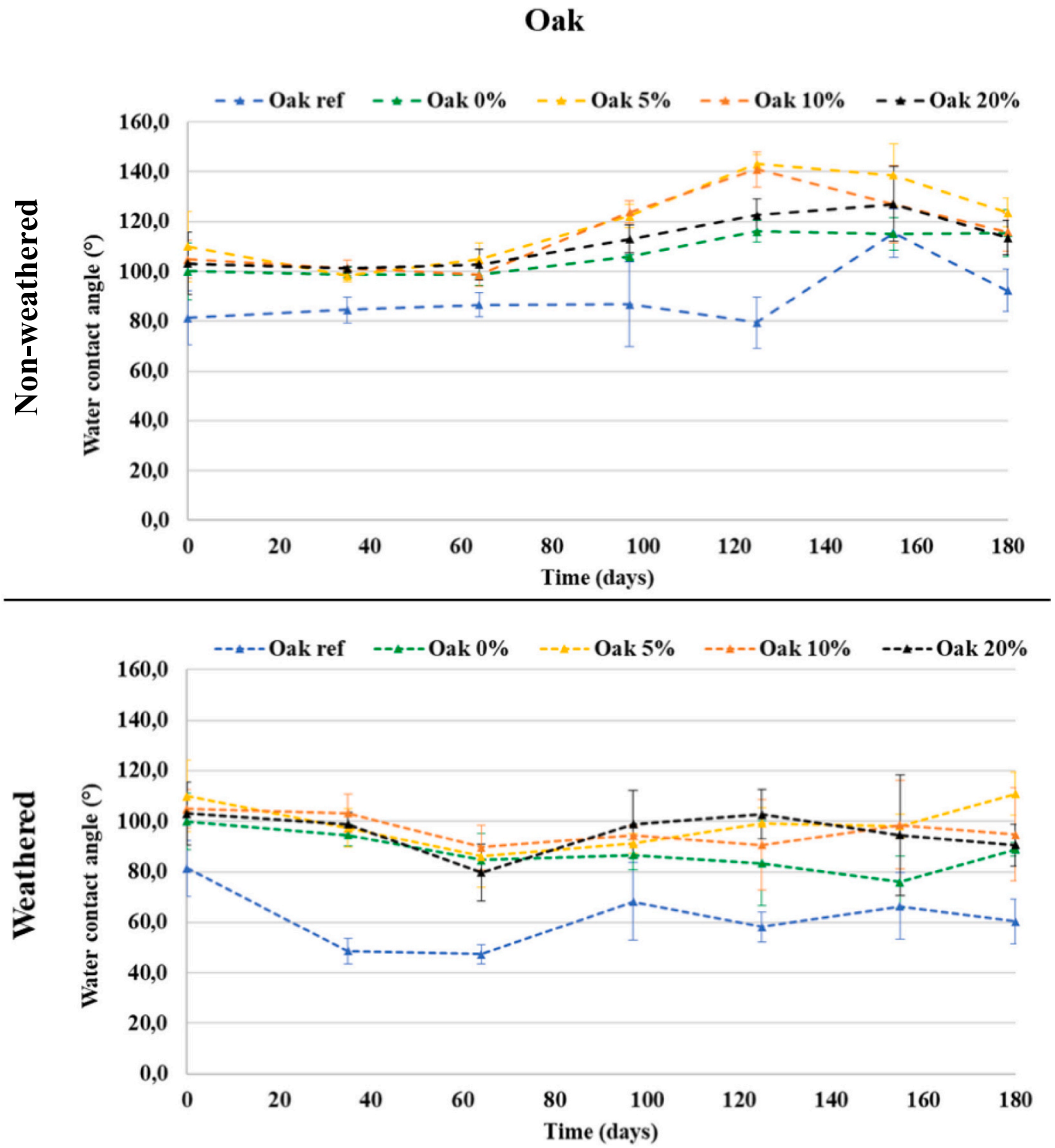

Fig. 9. Evolution of the water contact angle for non-weathered and weathered oak coatings with onsite weathering time. Figure in colour online only.

oil, both surfaces gained a hydrophobic property and achieved 101° and 100° at day 0 for beech and oak, respectively. Janesh et al. [45] successfully used tung oil on spruce wood boards to provide water resistance and reported a WCA increase by up to 48 %, going from 45° ± 9° to 88° ± 3° for the uncoated and coated surface, respectively. The water repellence for the non-weathered samples tended to increase over time as tung oil is a drying oil that keeps crosslinking over time, even if the surface was optically dry already at day 0.

BC/tung oil-coated wooden surfaces displayed increased hydrophobicity, presenting higher WCA values compared to specimens coated with tung oil only. However, the increase in biocarbon content was not correlated with an increase in WCA, since the highest WCA was close to super-hydrophobic values for 5 % BC for both oak (143°) and beech (135°), and no further improvement in hydrophobicity was observed either with 10 or 20 % BC. The achieved hydrophobicity of the biocarbon/tung oil coatings can be attributed to the synergetic effect of tung oil and the increased surface roughness brought on by the carbon particles. Indeed, according to the Wenzel model's assumption [46], the coating droplets penetrate more easily into the pores developed in a rough surface, which provides higher adhesive forces and increases the protective effect of the coating against water (i.e. its hydrophobicity). Additionally, the hydrophobic nature of BC [47], previously highlighted by the moisture content measured by proximate analysis (comprised between 1.65 and 2.50 wt% [24]), contributed to the overall hydrophobicity of the developed coatings. WCA values were similar for coated beech and oak at equivalent BC content and weathering time, which means that the wooden surface type did not affect the efficiency of the coating.

The weathering negatively affected the water repellence of all the samples considered in the study (control samples and coated samples with various BC content). However, the decrease in water repellence was not proportional to the weathering time. This observation can result from the combination of several phenomena. Firstly, upon exposition to onsite weathering, the sample's surface undergoes the effects of combined sun and rain. This weathering induces both degradation of the wood's hydrophobic components, such as lignin, under UV light and water and leaching of their hydrophobic derivatives (esters, quinones and ketones), which makes the wood surface richer in hydrophilic holocellulose [46]. Moreover, the microcracks formed during weathering could favor water penetration and degradation of the surface [35].

These alterations will tend to decrease water repellence. Secondly, the tung oil kept crosslinking over time, which increased the water repellence for the weathered samples over time. Thirdly, the onsite weathering induced unpredictable weather conditions. Hence, the 24 h of conditioning prior to monthly measurements might not be sufficient for the wooden surfaces to be completely dry and ensure systematic equal conditions.

Overall, the maximum decrease in water repellence for the reference and coatings containing 0 to 10 % BC was measured between 37 and 51 % for beech, and between 31 and 50 % for oak, respectively. The coatings containing 20 % BC performed the best, with a maximum decrease in water repellence reaching 25 and 26 % for beech and oak respectively. Hence, introducing a sufficient amount of BC limited the decrease in water repellence induced by the onsite weathering.

4. Conclusions

The absorbance of water solutions containing the dispersed BC particles, investigated in this study as UV absorbers, was roughly constant in the UV and visible range, and was directly proportional to the concentration of the solution. Even if the FTIR spectra of BC powders carbonized at different temperatures highlighted differences in the functional groups, no clear relationship was found between the production process parameters of the BC and their absorbance.

Cross sections of coated beech and oak surfaces highlighted very little penetration of the coating (<0.5 mm) and showed that the penetration occurred through earlywood vessels. Despite poor penetration, the surface coating visually appeared with microscope observation to have protected the surface from degradation. Uncoated samples and tung oil-coated beech and oak substrates without BC had an increase in the total colour change over weathering time, indicating an evident alteration of the wood surface aesthetics. Beech was more affected than oak due to the differences in the composition of these two wood species. An increased BC content in the coatings led to enhanced colour stability, with alteration of the colour close to 2 for both wood species after six months of weathering for 10 and 20 wt% BC, meaning that the colour change is only perceptible through close observation.

Regarding the wettability of the surfaces, initially, both uncoated (reference) beech and oak surfaces showed a hydrophilic character. After treatment with tung oil, both surfaces gained a hydrophobic property. The introduction of BC induced an increase in hydrophobicity compared to specimens coated with tung oil only. However, the increase in BC content was not correlated with increased water repellence. The highest water contact angle was observed for the 5 % BC samples, and no further improvement in hydrophobicity was observed with higher BC content. The weathering negatively affected the water repellence of all the samples considered in the study (i.e., reference and coated samples with various BC content). However, the introduction of 20 % BC best protected the decrease in water repellence induced by the onsite weathering.

Overall, the sustainable coatings developed in this study showed promising properties for protecting wooden surfaces in façades or other outdoor applications. The coatings with the highest BC content (20 wt% in tung oil) led to the least total colour change and preserved most of the water repellence of the coatings after 6-months of onsite weathering.

Since the absorbance of BC particles was found to be proportional to their concentration, and the smallest the particles, the highest the absorbance, further research using nanosized BC particles is warranted. This approach could simultaneously allow decreasing the BC content for an equal efficiency, thus opening new paths toward clearer coating for a better appreciation of the wood grain.

Funding

This work was supported by the European Union's Horizon 2020 research and innovation programme under the Marie Sklodowska-Curie Actions [grant number 898179], the European Union's Horizon 2020 research and innovation programme under H2020-WIDESPREAD-2018-2020-6 [grant agreement No 952395], and H2020 WIDESPREAD-2-Teaming [grant number 739574] and investment from the Republic of Slovenia and the European Regional Development Fund.

CRediT authorship contribution statement

L.M.: Conceptualization; Data curation; Funding acquisition; Investigation; Methodology; Writing - original draft. M.Z.: Data curation; Investigation; Writing - original draft. M.S.: Data curation; Investigation; Writing - review & editing. D.B.D.: Conceptualization; Funding acquisition; Supervision; Writing - review & editing. All authors have read and agreed to the published version of the manuscript.

Declaration of competing interest

The authors declare that they have no known competing financial interests or personal relationships that could have appeared to influence the work reported in this paper.

Data availability

Data will be made available on request.

Appendix A. Supplementary data

Supplementary data to this article can be found online at https://doi.org/10.1016/j.porgcoat.2023.107428.

References

[1] C.-D. Varganici, L. Rosu, D. Rosu, F. Mustata, T. Rusu, Sustainable wood coatings made of epoxidized vegetable oils for ultraviolet protection, Environ. Chem. Lett. 19 (2021) 307–328, https://doi.org/10.1007/s10311-020-01067-w.
[2] L. Rosu, C. Varganici, F. Mustata, D. Rosu, I. Rosca, T. Rusu, Epoxy coatings based on modified vegetable oils for wood surface protection against fungal degradation, ACS Appl. Mater. Interfaces 12 (2020) 14443–14458, https://doi.org/10.1021/acsami.0c00682.
[3] L. Rosu, F. Mustata, C. Varganici, D. Rosu, T. Rusu, I. Rosca, Thermal behaviour and fungi resistance of composites based on wood and natural and synthetic epoxy resins cured with maleopimaric acid, Polym. Degrad. Stab. 160 (2019) 148–161, https://doi.org/10.1016/j.polymdegradstab. 2018.12.022.
[4] Y. Huang, J.C.-F. Law, T.-K. Lam, K.S.-Y. Leung, Risks of organic UV filters: a review of environmental and human health concern studies, Sci. Total Environ. 755 (2021), 142486, https://doi.org/10.1016/j.scitotenv.2020.142486.
[5] P.A. Christensen, A. Dilks, T.A. Egerton, J. Temperley, Infrared spectroscopic evaluation of the photodegradation of paint part I the UV degradation of acrylic films pigmented with titanium dioxide, J. Mater. Sci. 34 (1999) 5689–5700, https://doi.org/10.1023/A:1004737630399.
[6] V.T. Wallder, W.J. Clarke, J.B. DeCoste, J.B. Howard, Weathering studies on polyethylene, Industrial & Engineering Chemistry. 42 (1950) 2320–2325.
[7] M. Liu, A.R. Horrocks, Effect of carbon black on UV stability of LLDPE films under artificial weathering conditions, Polym. Degrad. Stab. 75 (2002) 485–499, https://doi.org/10.1016/S0141-3910(01)00252-X.
[8] H. Schonhorn, J.P. Luongo, Effect of fillers on the photooxidative stabilization of polyethylene, Macromolecules 2 (1969) 364–366, https://doi.org/10.1021/ma60010a009.
[9] R. Chennareddy, H. Tuwair, U.F. Kandil, M. ElGawady, M.M. Reda Taha, UV-resistant GFRP composite using carbon nanotubes, Constr. Build. Mater. 220 (2019) 679–689, https://doi.org/10.1016/j.conbuildmat.2019.05.167.
[10] B. Yuan, M. Guo, Z. Huang, N. Naik, Q. Hu, Z. Guo, A UV-shielding and hydrophobic graphitic carbon nitride nanosheets/cellulose nanofibril (gCNNS/CNF) transparent coating on wood surface for weathering resistance, Prog. Org. Coat. 159 (2021), 106440, https://doi.org/10.1016/j.porgcoat.2021.106440.
[11] D. Łukawski, A. Lekawa-Raus, F. Lisiecki, K. Koziol, A. Dudkowiak, Towards the development of superhydrophobic carbon nanomaterial coatings on wood, Prog. Org. Coat. 125 (2018) 23–31, https://doi.org/10.1016/j.porgcoat.2018.08.025.
[12] Biomass Gasification, Pyrolysis and Torrefaction, Elsevier, 2013, https://doi.org/10.1016/C2011-0-07564-6.
[13] C. Zhang, G. Zeng, D. Huang, C. Lai, M. Chen, M. Cheng, W. Tang, L. Tang, H. Dong, B. Huang, X. Tan, R. Wang, Biochar for environmental management: mitigating greenhouse gas emissions, contaminant treatment, and potential negative impacts, Chem. Eng. J. 373 (2019) 902–922, https://doi.org/10.1016/j.cej.2019.05.139.

[14] L. Yang, G. Chen, N. Zhang, Y. Xu, X. Xu, Sustainable biochar-based solar absorbers for high-performance solar-driven steam generation and water purification, ACS Sustain. Chem. Eng. 7 (2019) 19311–19320, https://doi.org/10.1021/acssuschemeng.9b06169.
[15] Z. Li, C. Wang, T. Lei, H. Ma, J. Su, S. Ling, W. Wang, Arched bamboo charcoal as interfacial solar steam generation integrative device with enhanced water purification capacity, Adv. Sustain. Syst. 3 (2019) 1800144, https://doi.org/10.1002/adsu.201800144.
[16] Q. Fang, T. Li, Z. Chen, H. Lin, P. Wang, F. Liu, Full biomass-derived solar stills for robust and stable evaporation to collect clean water from various water-bearing media, ACS Appl. Mater. Interfaces 11 (2019) 10672–10679, https://doi.org/10.1021/acsami.9b00291.
[17] H. Jiang, X. Geng, S. Li, H. Tu, J. Wang, L. Bao, P. Yang, Y. Wan, Multi-3D hierarchical biomass-based carbon particles absorber for solar desalination and thermoelectric power generator, J. Mater. Sci. Technol. 59 (2020) 180–188, https://doi.org/10.1016/j.jmst.2020.05.023.
[18] H.M. Wilson, D.J. Ahirrao, S. Raheman Ar, N. Jha, Biomass-derived porous carbon for excellent low intensity solar steam generation and seawater desalination, Sol. Energy Mater. Sol. Cells 215 (2020), 110604, https://doi.org/10.1016/j.solmat.2020.110604.
[19] T.G. Chatzimitakos, A. Kasouni, A. Troganis, I. Leonardos, I. Tzovenis, A. Ntzouvaras, C. Stalikas, Carbon nanodots synthesized from Dunaliella Salina as sun protection filters, C. 6 (2020) 69, https://doi.org/10.3390/c6040069.
[20] B. Arminger, J. Jaxel, M. Bacher, W. Gindl-Altmutter, C. Hansmann, On the drying behavior of natural oils used for solid wood finishing, Prog. Org. Coat. 148 (2020), 105831, https://doi.org/10.1016/j.porgcoat.2020.105831.
[21] M. Humar, B. Lesar, Efficacy of linseed- and tung-oil-treated wood against wood-decay fungi and water uptake, Int. Biodeterior. Biodegrad. 85 (2013) 223–227, https://doi.org/10.1016/j.ibiod.2013.07.011.
[22] X. Yang, S. Zhang, W. Li, The performance of biodegradable tung oil coatings, Prog. Org. Coat. 85 (2015) 216–220, https://doi.org/10.1016/j.porgcoat.2015.04.015.
[23] S.C. Peterson, M.A. Jackson, S. Kim, D.E. Palmquist, Increasing biochar surface area: optimization of ball milling parameters, Powder Technol. 228 (2012) 115–120, https://doi.org/10.1016/j.powtec.2012.05.005.
[24] L. Marrot, K. Candelier, J. Valette, C. Lanvin, B. Horvat, L. Legan, D.B. DeVallance, Valorization of hemp stalk waste through thermochemical conversion for energy and electrical applications, Waste Biomass Valoriz. 13 (2022) 2267–2285, https://doi.org/10.1007/s12649-021-01640-6.
[25] N. Nan, D.B. DeVallance, Development of poly(vinyl alcohol)/wood-derived biochar composites for use in pressure sensor applications, J. Mater. Sci. 52 (2017) 8247–8257, https://doi.org/10.1007/s10853-017-1040-7.
[26] B. Zhao, D. O'Connor, J. Zhang, T. Peng, Z. Shen, D.C.W. Tsang, D. Hou, Effect of pyrolysis temperature, heating rate, and residence time on rapeseed stem derived biochar, J. Clean. Prod. 174 (2018) 977–987, https://doi.org/10.1016/j.jclepro.2017.11.013.
[27] S. Ebrahimzadeh Omran, M. Shorafa, A.A. Zolfaghari, A.A. Soltani Toolarood, The effect of biochar on severity of soil water repellency of crude oil-contaminated soil, Environ. Sci. Pollut. Res. 27 (2020) 6022–6032, https://doi.org/10.1007/s11356-019-07246-9.
[28] D. Kotaiah Naik, K. Monika, S. Prabhakar, R. Parthasarathy, B. Satyavathi, Pyrolysis of sorghum bagasse biomass into bio-char and bio-oil products: a thorough physicochemical characterization, J. Therm. Anal. Calorim. 127 (2017) 1277–1289, https://doi.org/10.1007/s10973-016-6061-y.
[29] Y. Zhao, L. Huang, Y. Chen, Biochars derived from giant reed (Arundo donax L.) with different treatment: characterization and ammonium adsorption potential, Environ. Sci. Pollut. Res. 24 (2017) 25889–25898, https://doi.org/10.1007/s11356-017-0110-3.
[30] R. Janu, V. Mrlik, D. Ribitsch, J. Hofman, P. Sedláček, L. Bielská, G. Soja, Biochar surface functional groups as affected by biomass feedstock, biochar composition and pyrolysis temperature, Carbon Resour. Convers. 4 (2021) 36–46, https://doi.org/10.1016/j.crcon.2021.01.003.
[31] M.K. Hossain, V. Strezov, K.Y. Chan, A. Ziolkowski, P.F. Nelson, Influence of pyrolysis temperature on production and nutrient properties of wastewater sludge biochar, J. Environ. Manag. 92 (2011) 223–228, https://doi.org/10.1016/j.jenvman.2010.09.008.
[32] S. Nanda, P. Mohanty, K. Pant, S. Naik, J. Kozinski, A. Dalai, Characterization of north american lignocellulosic biomass and biochars in terms of their candidacy for alternate renewable fuels, BioEnergy Res. 6 (2012), https://doi.org/10.1007/s12155-012-9281-4.
[33] D. Angın, Effect of pyrolysis temperature and heating rate on biochar obtained from pyrolysis of safflower seed press cake, Bioresour. Technol. 128 (2013) 593–597, https://doi.org/10.1016/j.biortech.2012.10.150.
[34] F. Shafizadeh, Pyrolytic reactions and products of biomass, in: R.P. Overend, T. A. Milne, L.K. Mudge (Eds.), Fundam. Thermochem. Biomass Convers, Springer Netherlands, Dordrecht, 1985, pp. 183–217, https://doi.org/10.1007/978-94-009-4932-4_11.
[35] B. Kaczmarczyk, FTIR study of conjugation in selected aromatic polyazomethines, J. Mol. Struct. 1048 (2013) 179–184, https://doi.org/10.1016/j.molstruc.2013.05.036.
[36] M. Inyang, B. Gao, P. Pullammanappallil, W. Ding, A.R. Zimmerman, Biochar from anaerobically digested sugarcane bagasse, Bioresour. Technol. 101 (2010) 8868–8872, https://doi.org/10.1016/j.biortech.2010.06.088.
[37] T.C. Bond, R.W. Bergstrom, Light absorption by carbonaceous particles: an investigative review, Aerosol Sci. Technol. 40 (2006) 27–67, https://doi.org/10.1080/02786820500421521.
[38] L. Marrot, M. Zouari, B. Borin, D.B. DeVallance, Sustainable Anti-UV Coating to Protect Wooden Façades Using Biocarbon as UV-stabilizer, 2021, https://doi.org/10.5281/zenodo.6590092.
[39] Y. Peng, Y. Wang, R. Zhang, W. Wang, J. Cao, Improvement of wood against UV weathering and decay by using plant origin substances: tannin acid and tung oil, Ind. Crop. Prod. 168 (2021), 113606, https://doi.org/10.1016/j.indcrop.2021.113606.
[40] F. Poohphajai, J. Sandak, M. Sailer, L. Rautkari, T. Belt, A. Sandak, Bioinspired living coating system in service: evaluation of the wood protected with biofinish during one-year natural weathering, Coatings. 11 (2021) 701, https://doi.org/10.3390/coatings11060701.
[41] K.K. Pandey, A note on the influence of extractives on the photo-discoloration and photo-degradation of wood, Polym. Degrad. Stab. 87 (2005) 375–379, https://doi.org/10.1016/j.polymdegradstab. 2004.09.007.
[42] L. Persze, L. Tolvaj, Photodegradation of wood at elevated temperature: colour change, J. Photochem. Photobiol. B 108 (2012) 44–47, https://doi.org/10.1016/j.jphotobiol.2011.12.008.
[43] X. Wang, H. Ren, Comparative study of the photo-discoloration of moso bamboo (Phyllostachys pubescens Mazel) and two wood species, Appl. Surf. Sci. 254 (2008) 7029–7034, https://doi.org/10.1016/j.apsusc.2008.05.121.
[44] K.-Y. Law, Definitions for hydrophilicity, hydrophobicity, and superhydrophobicity: getting the basics right, J. Phys. Chem. Lett. 5 (2014) 686–688, https://doi.org/10.1021/jz402762h.
[45] J. Janesch, B. Arminger, W. Gindl-Altmutter, C. Hansmann, Superhydrophobic coatings on wood made of plant oil and natural wax, Prog. Org. Coat. 148 (2020), 105891, https://doi.org/10.1016/j.porgcoat.2020.105891.
[46] R.N. Wenzel, Surface roughness and contact angle, J. Phys. Colloid Chem. 53 (1949) 1466–1467, https://doi.org/10.1021/j150474a015.
[47] J. Mao, K. Zhang, B. Chen, Linking hydrophobicity of biochar to the water repellency and water holding capacity of biochar-amended soil, Environ. Pollut. 253 (2019) 779–789, https://doi.org/10.1016/j.envpol.2019.07.051.